Antibacterial Properties of Pure Silver Films with Nanoparticles Induced by Pulsed-Laser Dewetting Process

Y. H. Lin[1], J. J. Wang[2], Y. T. Wang[2], H. K. Lin[2,*], Y. J. Lin[1]

[1] Department of Plant Medicine, National Pingtung University of Science and Technology, Pingtung 912, Taiwan

[2] Graduate Institute of Materials Engineering, National Pingtung University of Science and Technology, Pingtung 912, Taiwan

* Corresponding author: E-mail: HKLin@mail.npust.edu.tw

Abstract

Silver particles are prepared by dewetting Ag films coated on glass using a fiber laser. The size of the particles is controlled in the range of 92 nm ~ 1.2 μm by adjusting the thickness of the Ag film. The structural properties and surface roughness of the particles are evaluated by means of scanning electron microscopy. In addition, the antifungal activity of the Ag particles is examined using spore suspensions of *Colletotrichum gloeosporioides*. It is shown that the particles with a size of 1.2 μm achieve 100% inhibition of the conidia growth of the *Colletotrichum gloeosporioides* after a contact time of just 5 min. Furthermore, the smaller particles also achieve a good antibacterial activity given a longer contact time. Similar results are observed in spore germination and pathogenicity tests performed on mango fruit and leaves. Overall, the results confirm that the Ag particles have an excellent antifungal effect on *Colletotrichum gloeosporioides*.

Keywords: Ag; Colletotrichum gloeosporioides; laser; dewetting

1. Introduction

Mango (*Mangifera indica* L.) is a popular fruit with a strong and distinctive flavor and is widely grown in many tropical and subtropical countries [1]. However, during the growth stage, the mango fruit and leaves are often affected by anthracnose disease, in which *Colletotrichum gloeosporioides* (*C. gloeosporioides*) fungi cause severe lesions with black spots. Some estimates have placed the incidence of anthracnose disease in farmer's fields as high as 36~74% [2].

Traditionally, *C. gloeosporioides* fungi are treated by chemical spraying. However, the fungi have gradually developed resistance to commercial fungicides, and hence alternative methods for combating anthracnose disease are required [3].

Metallic antimicrobial surfaces are widely used for the storage and delivery of water. For example, studies have shown that Ag bottles and vessels provide an effective means of preventing the spoilage of stored water by bacteria [4]. Furthermore, the surface chemistry modification of such surfaces, combined with proper cleaning products and procedures, produces a further improvement in the antimicrobial performance [5]. In recent years, the antifungal activity of nanoparticles (NPs) against some phytopathogenic fungi have been investigated [6]. Many studies have demonstrated the effectiveness of Ag, Cu and ZnO nanoparticles (NPs) in inhibiting the activity of phytopathogenic fungi [3, 7-9]. Ag NPs show a particularly strong bactericidal performance. The textile with silver additions has antimicrobial activities, meanwhile, thin films coated on the substrate have antifungal function. Chowdappa [10] reported that chitosan-AgNP composite exhibits a higher antifungal activity against *C. gloeosporioides* than its components [11]. The biological activity of metallic glass materials has also attracted significant attention in recent years [12, 13]. Chen [14] reported that the growth area of microbes on Zr-based metallic glass films was smaller than that on SUS304 substrates. Furthermore, the coatings exhibit a particularly long-term antimicrobial effect for P. aeruginosa. The TFMGs extend attainable size of the metallic glass and show a potential application in medical related field.

Nowadays, most applications on plant pathogens use nanomaterials as fungicides [15]. Studies have shown that Cu nanoparticles inhibit plant pathogens such as *phoma destructiva*, *curvularia lunata* and *alternaria*, while Ag particles suppress the growth of *macrophomina phaseolina* and *rhizoctonia solani* [7]. Therefore, nanoparticles have potential for development as a bacteriostatic or fungicide. Various techniques are available for the production of micro- and nanoscale metallic particles, including mechanochemical methods [16], green synthesis [17], spray pyrolysis [18], sol-gel [19], chemical vapor deposition [20], and dewetting [21]. In the latter method,

a metallic film is deposited on a glass substrate and is then annealed; resulting in a dewetting phenomenon which minimizes the total energy of the free surfaces of the film and substrate. Compared to other methods, dewetting has the advantages of large area coverage, low cost, and the production of ordered NPs. Furthermore, the rapid thermal treatment of thin Ag/Cu bilayers also enables the production of composite Ag-Cu nanoparticles [22]. However, the high melting temperatures of most metals are not easily achievable using conventional heating methods. Therefore, the dewetting process is generally performed using high-energy sources such as focused ion beams and lasers [23].

The feasibility of pulsed laser-induced dewetting, especially that using nanosecond pulses, has attracted significant attention in the literature [24-27]. However, only scant information is available regarding the synthesis of metallic NPs using a high repetition rate laser. Accordingly, the present study prepares Ag particles with various sizes using a high repetition rate pulsed laser and an Ag film with a carefully controlled thickness. The antifungal activity of the Ag particles is investigated by examining the conidia growth and germination rate of *C. gloeosporioides* spores in both *in vitro* experiments and *in vivo* experiments performed using mango fruit and leaves.

2. Experiment

2.1 Silver particle preparation

Glass substrates (AGC G2, 150 mm×150 mm x 0.7 mm) were cleaned ultrasonically in deionized water for 15 min. The substrates were dried with hot air and then transferred to an SSI-T500-1 thermal evaporator system. The base pressure of the evaporation chamber was set as 6×10^{-6} Torr prior to the thermal evaporation process. Silver pellets (Ultimate Materilas Technology Co., Taiwan) were loaded into a tungsten boat in the evaporation chamber and vaporized by a resistive heat source. The growth conditions of the Ag film on the glass substrate were controlled by adjusting the current (I_{Ag}) and time of the evaporation process. In particular, I_{Ag} was fixed at 60 A and the time was adjusted as required to produce Ag thin films with thicknesses of 10 nm and 50

nm, respectively. The as-deposited films were dewetted using a fiber laser (SPI-12, UK, wavelength 1064 nm) with repetition rates ranging from 100 ~ 400 kHz and irradiation powers in the range of 8 ~ 12.5 W. For all of the samples, the laser spot size and pulse duration were set as 40 μm and 30 ns, respectively. Moreover, the laser scanning speed was varied in the range of 25 ~ 1200 mm/s. The pulse energy (E) was computed as [28]

$$E = P_{AVG} / rep, \tag{1}$$

where P_{AVG} is the average power of the pulse laser and *rep* is the laser repetition rate. From Eq. (1), it is seen that the pulse energy reduces as the repetition rate increases. For the irradiation powers and repetition rates considered in the present study, the pulse energy varied from 5 to 250 μJ. The shape, size and cross-sectional height of the Ag particles produced in the laser dewetting process were observed by an optical microscope (OM, HRM-300) and a scanning electron microscope (SEM, JSM-7600F). The wettability of the different samples was evaluated using a contact angle measurement system (OCA 15EC, Dataphysics). Finally, the surface roughness was measured using a surface roughness analyzer (Alpha-Step, KLA D-300) based on five separate measurements obtained under a load of 80 mg each time.

2.2 Antifungal test

Pathogenic *C. gloeosporioides* isolate (NCBI accession number KP900284.1) was cultured in potato dextrose broth (PDB) at 28°C for 7 days. After incubation, *C. gloeosporioides* spores were harvested by centrifugation (Heraeus™ Pico™ 17 Microcentrifuge, Thermo Scientific, Massachusetts, USA) at 13,000 rpm for 5 min and re-suspended in ddH_2O. 2-μl drops of the spore suspension were placed on a slide and the number of spore colonies was counted under a microscope. To assess the antifungal activity of the Ag particles, 150-μl spore suspensions of *C. gloeosporioides* were transferred with a micropipette to contact with the particles for 1, 5, 10 and 15 min, respectively. The spore suspensions were then transferred to potato dextrose agar (PDA) medium to evaluate the colony-forming units (CFUs) after 48 h incubation at 28°C. The antifungal efficacy (AE) of each sample was evaluated as [1- (A − B)] × 100, where A is the number of CFUs

following contact with the Ag particles and B is the number of CFUs following contact with an uncoated glass slide (control).

2.3 Spore germination inhibition assay

The possible antifungal mechanism of the NPs was investigated by means of spore germination inhibition assays. Aliquots of *C. gloeosporioides* spore suspension were contacted with Ag NPs for 1 and 15 min, respectively. 20-µl spore suspensions from each condition were transferred to glass slides, which were then incubated at 25°C. After 4, 8, 12, 24 and 48 h incubation, the spore germination was observed under a microscope and the percentage of spore germination was calculated. The spore germination rate (%) was calculated as [A/B] × 100, were A is the number of CFUs for the Ag sample and B is the number of CFUs for the control sample.

2.4 Morphology analysis

Disks of *C. gloeosporioides* (1 cm) and spores treated with Ag particles and glass were cultured in PDA medium and distilled water, respectively, in darkness at 28°C for every day. The colony count, hyphal morphology and mycelial radial growth rate were examined every day. In addition, the appressorium formation of each sample was observed at 0, 2, 4, 6 and 8 h after inoculation.

2.5 Virulence assay

Semi-ripe fruits of the mango cultivar 'Irwin' were prepared with weights of approximately 300 g. The fruits were washed in tap water, sterilized with 75% alcohol, and then washed twice with sterile distilled water. The fruits were then placed in a laminar air flow and dried under UV light for 10 minutes. Following the drying process, the samples were punctured on the same side to a depth of 2 mm with a sterilized needle. 20-µl *C. gloeosporioides* spore suspensions ($2*10^4$ conidia) were prepared and contacted with the Ag particle and glass (control) samples for 15 min. The wound and non-wound sites of the samples were then inoculated with 5-µl spore suspensions ($5*10^3$ conidia). The fruits were placed in a sterilized plastic box (40 x 20 x 45 cm) with 100% relative humidity

(RH) and incubated at 28°C for 7 days. Finally, the lesion lengths at each inoculation site were measured using an optical microscope.

2.6 RT-PCR analysis of gene expression

The effect of the Ag particles on the melanin synthesis behavior of the *C. gloeosporioides* spores was evaluated by performing the RT-PCT analysis of five related genes, namely polyketide synthase (PKS), tetra-HN reductase scytalone (THR), scytalone dehydratase (SCD), exo-glucocanase (Ecg) and pectate lyase (PEL). Seven primers were designed for the RT-PCR analysis, and 18S rRNA was selected as the internal control [29]. The RNA of the spores contacted with the different Ag particles and glass (control) sample for 15 min were extracted using an RNA purification kit (BIO-GENESIS, Germany). cDNA synthesis was then performed using a commercial reverse transcription system (Magic RT Mastermix cDNA synthesis kit, BIO-GENESIS, Germany). Finally, the cDNA was used for real-time quantitative PCR tests with the following program: 50 cycles at 95°C for 10 s, 60°C for 20 s, and 97°C for 60 s.

2.7 Morphology of *C. gloeosporioides* conidia

To observe the effect of the Ag particles on the morphology of the *C. gloeosporioides* conidia, conidia samples (109 conidia/ml) were contacted with the Ag particles with a size of 1.2 μm for 3 h and were then centrifuged at 13,300 rpm for 2 min. The resulting pellets were washed with sterile water and pre-fixed with 2.5% glutaraldehyde for 2 h. The pre-fixed cells were washed with phosphate buffered saline (PBS) two times and post-fixed with 1% osmium tetroxide for 1 h. After washing with PBS three times, a dehydration process was conducted with 30, 50, 70, 80, 90 and 100% of ethanol. Finally, the fixed cells were dried and gold-coated using an ion sputtering system (HITACHI HUS-SGB, Japan) and their morphology was observed by SEM (HITACHI S-3000N, Japan). Three replications were performed for each sample. All data were statistical analysis using analysis of variance (ANOVA) test. In addition, the means of the various samples were compared by a Tukey-HSD test （P = 0.05） and Fisher's Least Significant Difference (LSD) test （P <

0.01）．All of the analyses were performed using commercial statistical software (SPSS V. 20, IBM).

3. Results and Discussion

Figure 1 presents SEM images of the synthesized Ag particles. It is seen that the particle size increases with an increasing Ag film thickness and laser repetition rate. Moreover, from Fig. 2, the corresponding particle heights are 76 nm, 288 nm and 515 nm, respectively.

Figure 3 shows the relationship between the scanning speed and the laser input energy for initial Ag film thicknesses of 10 nm and 50 nm, respectively. As shown, both figures contain three distinct regions. In Region I, characterized by a low laser energy and high scanning speed, the energy is insufficient to prompt dewetting of the Ag film. As the scanning speed and laser energy increase, the input energy also increases and hence dewetting occurs; resulting in the formation of Ag particles (Region II). However, at excessive laser energies and low scanning speeds (Region III), the input energy leads to the ablation of the Ag film rather than dewetting, and consequently, no particles are formed. In general, the results confirm that the dewetting process is strongly dependent on the laser power and scanning speed. In particular, for a given scanning speed, a high laser energy results in the ablation of the Ag film, while a low laser energy results in an Ag film with many isolated island structures. For a constant laser energy, the particles tend to become larger with an increasing scanning speed due to a corresponding reduction in the thermal energy accumulation. It is noted that this finding is consistent with that reported in previous studies [30, 31]. The results presented in Fig. 3 confirm that the size of the particles produced in the dewetting process also depends on the thickness of the original Ag film. For a thicker film, the dewetting process can be performed at a higher energy, and particles with a micrometer scale are produced at all the corresponding scanning speeds. For a thinner film, particles can be obtained at a lower energy, and the particle size (nanometer) depends on the particular scanning speed applied [32]. Overall, the results show that the particle size decreases with an increasing laser energy and a decreasing film

thickness.

Table 1 shows the surface roughness (Ra) and contact angle measurements of the various Ag samples. The surface roughness increases with an increasing particle size as a result of the greater particle height (see Fig. 2). The contact angle also increases with an increasing particle size. For example, the particles with a size of 92 nm and 1.2 μm have contact angles of 43° and 73°, respectively. The surface roughness is another factor to affect the biological activities, suggesting that microbes are difficult to attach and move on an ultra-smooth surface [14]. Figure 4 presents OM images showing the conidia growth of the *C. gloeosporioides* spores contacted with the different samples. In general, the results show that the treated samples (92 nm, 570 nm and 1.2 μm) have significantly higher bacteriostatic properties than the control (glass) sample. The Ag sample with the largest particle size (1.2 μm) achieves 100% bacteriostasis within a contact time of 5 min. For the sample with an Ag particle size of 570 nm, 100% bacteriostasis is also achieved. However, the contact time increases to 10 min. For the smallest particle size of 92 nm, the sample contains 22 colonies after 15 min. In other words, full bacteriostasis is not achieved. However, overall, the results confirm that the conidia growth suppression ability of all the samples increases with an increasing particle size and contact time. The present results are consistent with those of [33-35], which showed that metallic Ag has an excellent inhibitory ability against both bacteria (*escherichia coli*, *staphylococcus aureus* and *pseudomonas aeruginosa*) and fungi (f*usarium oxysporum* and *botrytis cinerea*).

Figure 5 shows the spore germination rates of the *C. gloeosporioides* contacted with the different Ag samples for periods of 1 min and 15 min, respectively. For both contact periods, the spore germination rates of the treated samples are significantly lower than those of the untreated sample. Furthermore, for the Ag samples, the germination rate decreases by around 20% as the contact time is increased from 1 to 15 min. The germination rate also decreases with an increasing particle size. For example, given a contact time of 15 min, the germination rate reduces from around 29% to 15% as the particle size increases from 92 nm to 1.2 μm. It is noted that this trend is

consistent with the plate test results (see Fig. 4). Anthrax appressorium formation is one of the most important structures invading the host [29]. Figure 6 presents OM images showing the appressorium formation of *C. gloeosporioides* spores contacted with the treated and untreated samples. For the untreated sample, germination is observed after 2 h of cultivation and the appressorium formation rate is equal to $40.2 \pm 6.2\%$ after 8 h. In addition, germ tube and appressorium formation are observed after 4 h and 6 h, respectively. However, for the treated samples, germ tube formation is not observed until 6 h of incubation. In addition, no appressorium formation is observed for any of the samples; even after 8 h. In other words, the results confirm the ability of the Ag particles to inhibit the formation of pathogenic anthrax bacteria.

Figure 7 shows the morphologies of the *C. gloeosporioides* spores treated with different Ag particles for 15 min and then incubated in PDA at 28°C for 6 days. Note that for each sample, the left and right images present front and rear views of the colony morphology, respectively. It is observed that the melanin precipitation in the treated samples is greatly reduced compared to that in the untreated (control) sample. Among the treated samples, the sample with a 1.2-μm particle size has a particularly low melanin precipitation. Wei [29] showed that anthrax bacteria produce melanin to accumulate the swell pressure inside the press. In other words, the amount of melanin is one of the key factors determining the pathogenic ability of anthrax bacteria. Overall, the results presented in Fig. 7 suggest that Ag particle treatment is effective in suppressing melanin expression and hence in limiting the activity of anthrax bacteria. Figure 8 shows the relative expressions of the LAC1, PKS, THR, SCD, Ecg and PEL genes following contact with the treated and un-treated samples. The results confirm that exposure to the Ag particles results in a significant reduction in the melanin synthesis compared to that for the untreated sample. Moreover, for each gene, the melanin synthesis reduces with an increasing particle size.

Figure 9 shows the effect of the Ag nanoparticles on the extent of the anthracnose of the mango samples. Compared to the control sample, the pathogenicity of the *C. gloeosporioides* conidia is notably reduced in the treated samples. The detailed inoculation results presented in

Table 2 show that the lesion size reduces from 13.50 mm to 11.00 nm as the Ag particle size increases from 92 nm to 1.2 μm. In other words, the results are consistent with those of the plate bacteriostatic and spore germination tests, which show that the Ag sample with a particle size of 1.2 μm has particularly good bacteriostatic properties and a superior suppression ability of *C. gloeosporio*ides.

Figure 10 presents SEM images showing the morphologies of the *C. gloeosporioides* conidia following contact with the untreated control sample and the sample with an Ag particle size of 1.2 μm. The *C. gloeosporioides* conidia of the untreated sample have an oval cell-like appearance with a smooth surface. By contrast, for the treated sample, the conidia surfaces contain small irregular fragments; indicating that exposure to the Ag particles results in damage to the cell surface, and hence inhibits the invasion and growth of the *C. gloeosporioides* spores during incubation.

4. Conclusion

Silver particles have been prepared on glass slides using a combined thermal evaporation and laser dewetting process. It has been shown that the size of the particles can be controlled in the range of 92 nm ~ 1.2 μm by adjusting the thickness of the Ag film deposited on the glass slide and the laser energy applied during the dewetting process. The antibacterial performance of the Ag samples has been investigated by examining the conidia growth of *C. gloeosporioides*; a fungus spore associated with the anthracnose disease of mango. The results have shown that the conidia growth suppression effect increases with an increasing Ag particle size and contact time. For the largest particle size of 1.2 μm, 100% bacteriostasis is achieved within a contact time of 5 min. Furthermore, even for the smallest particle size (92 nm), a strong antibacterial performance is also observed after a contact time of 15 min. A similar size-dependent effect is also observed in the spore germination and pathogenicity tests. Overall, the present results confirm that Ag particles have an excellent inhibitory ability on *C. gloeosporioides*.

Acknowledgements

Reference

[1] Khalid P. Akhtar, S.S. Alam, Assessment keys for some important Diseases of Mango, Pakistan Journal of Biological Science 5 (2002) 246-250.

[2] Ayantu Tucho, Fikre Lemessa, G. Berecha, Distribution and Occurrence of Mango Anthracnose (Colletotrichum gloesporioides Penz and Sacc) in Humid Agro-ecology of Southwest Ethiopia, Plant Pathology Journal 13 (2014) 268-277.

[3] L. He, Y. Liu, A. Mustapha, M. Lin, Antifungal activity of zinc oxide nanoparticles against Botrytis cinerea and Penicillium expansum, Microbiological research 166(3) (2011) 207-15.

[4] V. Villapún, L. Dover, A. Cross, S. González, Antibacterial Metallic Touch Surfaces, Materials 9(9) (2016) 736.

[5] C.H. Huang, Y.S. Huang, Y.S. Lin, C.H. Lin, J.C. Huang, C.H. Chen, J.B. Li, Y.H. Chen, J.S.C. Jang, Electrochemical and biocompatibility response of newly developed TiZr-based metallic glasses, Materials Science and Engineering: C 43 (2014) 343-349.

[6] Valionllah Mahdizadeh, Naser Safaie, F. Khelghatibana, Evaluation of antifungal activity of silver nanoparticles against some phytopathogenic fungi and Trichoderma harzianum, J. Crop Prot. 4 (2015) 291-300.

[7] A. Herman, A.P. Herman, Nanoparticles as Antimicrobial Agents: Their Toxicity and Mechanisms of Action, Journal of Nanoscience and Nanotechnology 14(1) (2014) 946-957.

[8] Soo-Hwan Kim, Hyeong-Seon Lee, Deok-Seon Ryu, Soo-Jae Choi, D.-S. Lee, Antibacterial Activity of Silver-nanoparticles Against Staphylococcus aureus and Escherichia coli, Korean Journal of Microbiology and Biotechnology 39 (2011) 77-85.

[9] C. Nie, Y. Yang, C. Cheng, L. Ma, J. Deng, L. Wang, C. Zhao, Bioinspired and biocompatible carbon nanotube-Ag nanohybrid coatings for robust antibacterial applications, Acta biomaterialia 51 (2017) 479-494.

[10] P. Chowdappa, Shivakumar Gowda, S.C. C, S. Madhura, Antifungal activity of chitosan-silver nanoparticle composite against Colletotrichum gloeosporioides associated with mango anthracnose, African Journal of Microbiology Research 8(17) (2014) 1803-1812.

[11] S. Chernousova, M. Epple, Silver as antibacterial agent: ion, nanoparticle, and metal, Angewandte Chemie 52(6) (2013) 1636-53.

[12] J.P. Chu, J.S.C. Jang, J.C. Huang, H.S. Chou, Y. Yang, J.C. Ye, Y.C. Wang, J.W. Lee, F.X. Liu, P.K. Liaw, Y.C. Chen, C.M. Lee, C.L. Li, C. Rullyani, Thin film metallic glasses: Unique properties and potential applications, Thin Solid Films 520(16) (2012) 5097-5122.

[13] J.C. Huang, J.P. Chu, J.S.C. Jang, Recent progress in metallic glasses in Taiwan, Intermetallics 17(12) (2009) 973-987.

[14] H.W. Chen, K.C. Hsu, Y.C. Chan, J.G. Duh, J.W. Lee, J.S.C. Jang, G.J. Chen, Antimicrobial properties of Zr–Cu–Al–Ag thin film metallic glass, Thin Solid Films 561 (2014) 98-101.

[15] P. Kanhed, S. Birla, S. Gaikwad, A. Gade, A.B. Seabra, O. Rubilar, N. Duran, M. Rai, In vitro antifungal efficacy of copper nanoparticles against selected crop pathogenic fungi, Materials Letters 115 (2014) 13-17.

[16] W. Janbua, T. Bongkarn, W. Vittayakorn, N. Vittayakorn, Direct synthesis and growth mechanism of metal molybdate (AMoO 4 ; A = Ca and Ba) fine particles via the mechanochemical method, Ceramics International 43 (2017) S435-S443.

[17] O. Velgosová, A. Mražíková, R. Marcinčáková, Influence of pH on green synthesis of Ag nanoparticles, Materials Letters 180 (2016) 336-339.

[18] N. Kumar, F. Alam, V. Dutta, Deposition of Ag and Au–Ag alloy nanoparticle films by spray pyrolysis technique with tuned plasmonic properties, Journal of Alloys and Compounds 585 (2014) 312-317.

[19] M. Raffi, J.I. Akhter, M.M. Hasan, Effect of annealing temperature on Ag nano-composite synthesized by sol–gel, Materials Chemistry and Physics 99(2) (2006) 405-409.

[20] J.-C. Bradley, S. Babu, B. Carroll, A. Mittal, A study of spatially coupled bipolar electrochemistry on the sub-micrometer scale: colloidal particles on surfaces and cylinders in nuclear-track etched membranes, Journal of Electroanalytical Chemistry 522(1) (2002) 75-85.

[21] Y. Oh, M. Lee, Single-pulse transformation of Ag thin film into nanoparticles via laser-induced dewetting, Applied Surface Science 399 (2017) 555-564.

[22] K. Kumar, P. Swaminathan, Role of silver nanoparticles in the dewetting behavior of copper thin films, Thin Solid Films 642 (2017) 364-369.

[23] D.P. Datta, A. Chettah, V. Siva, D. Kanjilal, P.K. Sahoo, Dewetting induced Au-Ge composite nanodot evolution in SiO2, Applied Surface Science 428 (2018) 676-683.

[24] Y. Oh, J. Lee, M. Lee, Fabrication of Ag-Au bimetallic nanoparticles by laser-induced dewetting of bilayer films, Applied Surface Science 434 (2018) 1293-1299.

[25] S.K. Maurya, Y. Uto, K. Kashihara, N. Yonekura, T. Nakajima, Rapid formation of nanostructures in Au films using a CO 2 laser, Applied Surface Science 427 (2018) 961-965.

[26] M. Heinz, V.V. Srabionyan, L.A. Avakyan, A.L. Bugaev, A.V. Skidanenko, S.Y. Kaptelinin, J. Ihlemann, J. Meinertz, C. Patzig, M. Dubiel, L.A. Bugaev, Formation of bimetallic gold-silver nanoparticles in glass by UV laser irradiation, Journal of Alloys and Compounds 767 (2018) 1253-1263.

[27] J.E. Kline, J.P. Leonard, Suppression of dewetting phenomena during excimer laser melting of thin metal films on SiO2, Thin Solid Films 488(1-2) (2005) 306-313.

[28] B.R. Benware, C.D. Macchietto, C.H. Moreno, J.J. Rocca, Demonstration of a high average power tabletop soft X-Ray Laser, Physical Review Letters 81 (1998) 5804-5807.

[29] Y. Wei, J. Pu, H. Zhang, Y. Liu, F. Zhou, K. Zhang, X. Liu, The laccase gene (LAC1) is essential for Colletotrichum gloeosporioides development and virulence on mango leaves and fruits, Physiological and Molecular Plant Pathology 99 (2017) 55-64.

[30] F. Leroy, Ł. Borowik, F. Cheynis, Y. Almadori, S. Curiotto, M. Trautmann, J.C. Barbé, P. Müller, How to control solid state dewetting: A short review, Surface Science Reports 71(2) (2016) 391-409.

[31] N. Gazit, L. Klinger, E. Rabkin, Chemically-induced solid-state dewetting of thin Au films, Acta Materialia 129 (2017) 300-311.

[32] R. Lo Savio, L. Repetto, P. Guida, E. Angeli, G. Firpo, A. Volpe, V. Ierardi, U. Valbusa, Control of the micrometric scale morphology of silicon nanowires through ion irradiation-induced metal dewetting, Solid State Communications 240 (2016) 41-45.

[33] S.M. Ouda, Antifungal activity of sliver and copper nanoparticles on two plant pathogens, Alternaria alternata and Botrytis cinerea, Research Journal of Microbiology 9 (1) (2014) 34-42.

[34] Y.Y. Chu, Y.S. Lin, C.M. Chang, J.K. Liu, C.H. Chen, J.C. Huang, Promising antimicrobial capability of thin film metallic glasses, Materials science & engineering. C, Materials for biological applications 36 (2014) 221-5.

[35] A. C, P. C, H.K. Handral, C. Kelmani R, Investigation of antifungal and anti-mycelium activities using biogenic nanoparticles: An eco-friendly approach, Environmental Nanotechnology, Monitoring & Management 5 (2016) 81-87.

Table Captions

Table 1 Roughness and contact angle measurements of different Ag particle samples.

Sample particle sizes	Film thickness	Roughness (Ra)	Contact angle(°)
	(nm)	(nm)	H_2O
Glass	-	0.32 ± 0.01	62.92 ± 1.70
92 nm	10	4.89 ± 2.02	43.33 ± 2.00
570 nm	50	43.99 ± 0.24	50.54 ± 2.02
1.2 μm	50	73.09 ± 3.44	73.09 ± 0.80

Table 2. Efficacy of different Ag particle samples for anthracnose treatment of mango.

Treatment	Lesion size (mm)	
	Wound made	Non-Wound made
Control (Glass)	15.56 ± 0.76^a	13.10 ± 0.91^a
92 nm	13.50 ± 0.66^b	7.00 ± 1.95^b
570 nm	11.75 ± 0.69^c	6.80 ± 1.42^b
1.2 μm	11.00 ± 0.66^c	3.30 ± 1.15^c

* significant differences at P = 0.05 (ANOVA, post-hoc Tukey-HSD test).
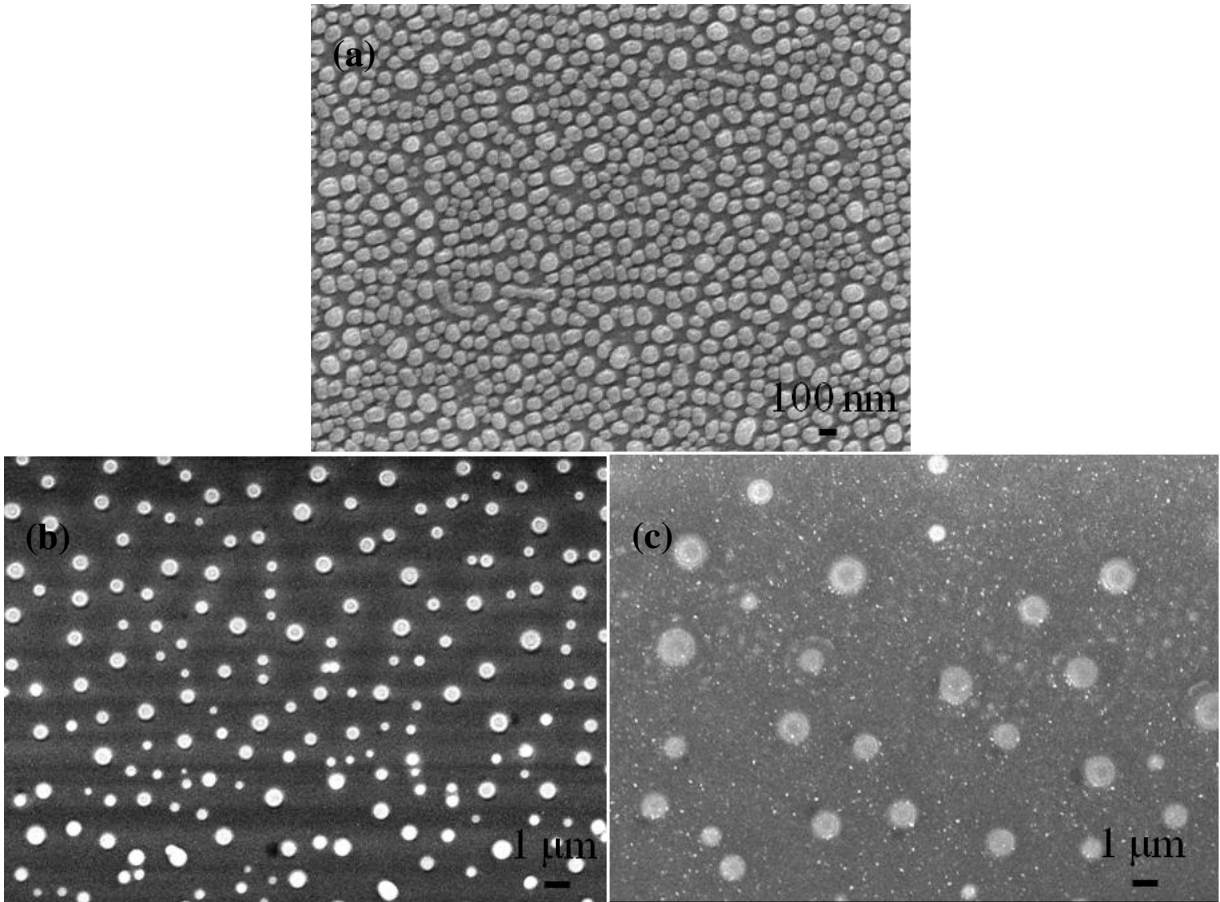
Figure Captions

Fig. 1 SEM images of Ag particles with a size of: (a) 92 nm, (b) 570 nm, and (c) 1.2 μm.

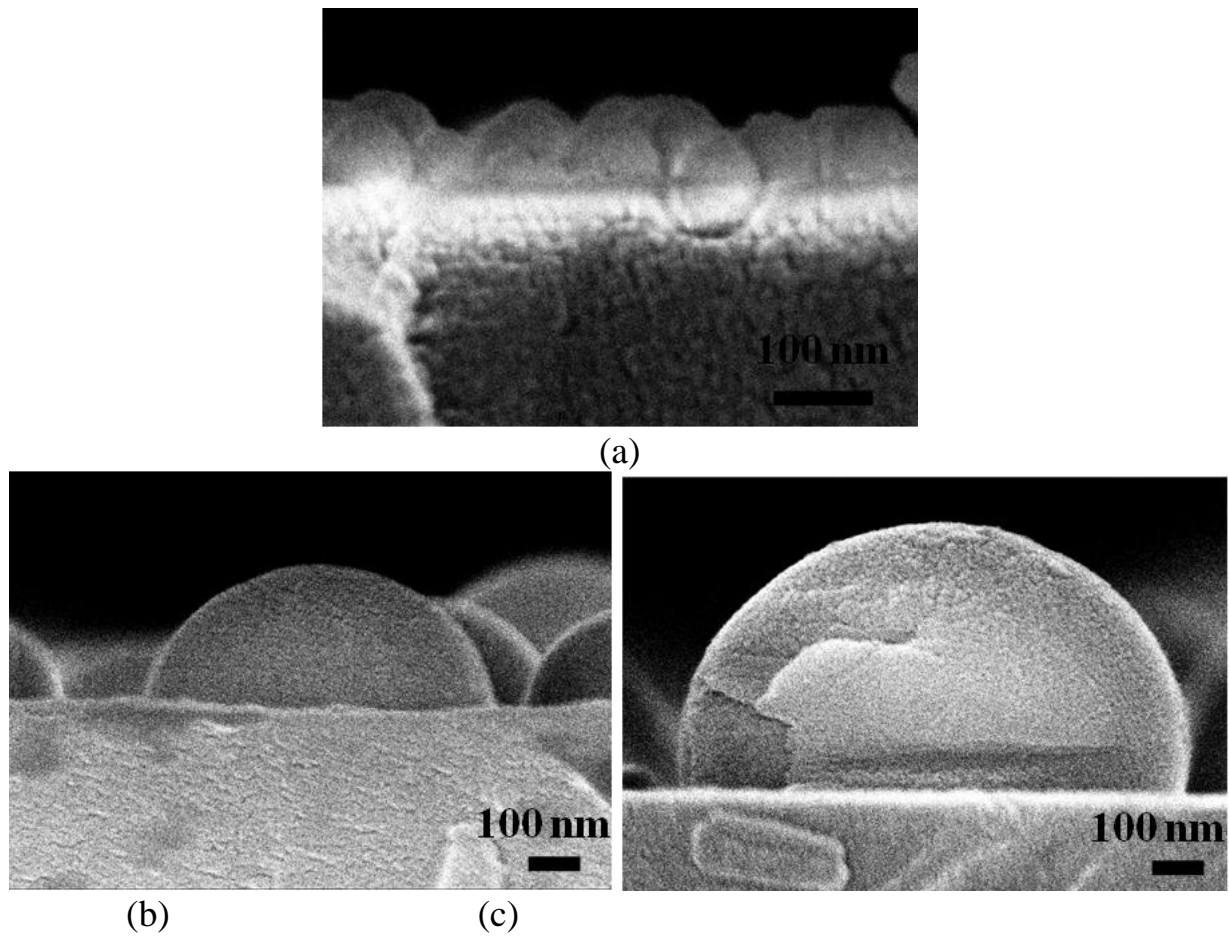Fig. 2 Cross-sectional images of Ag particles with different size of: (a) 92 nm, (b) 570 nm, and (c) 1.2 μm.
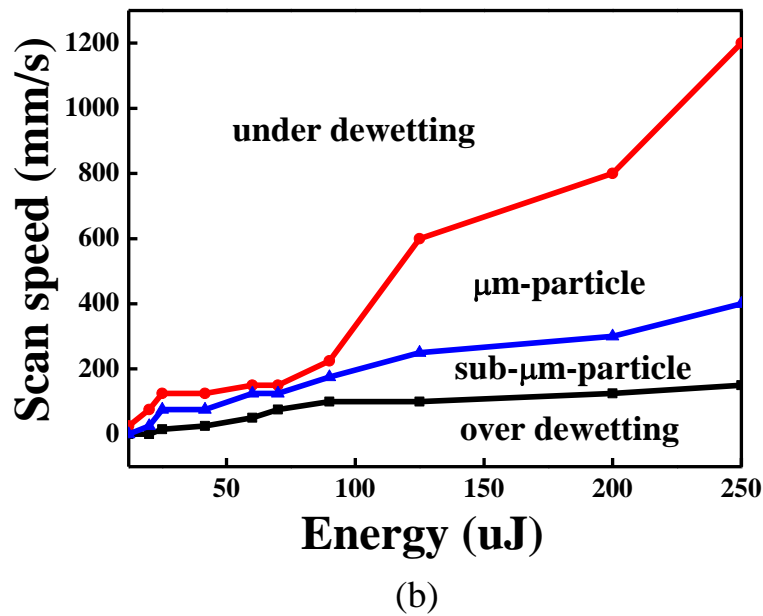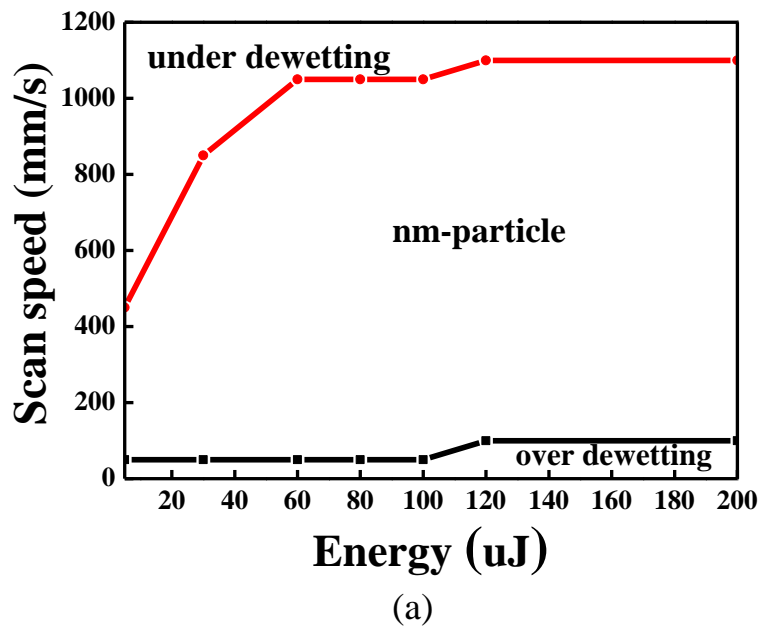
Fig. 3 Relationship between scanning speed and laser input energy for initial Ag film thickness of : (a) 10 nm and (b) 50 nm.
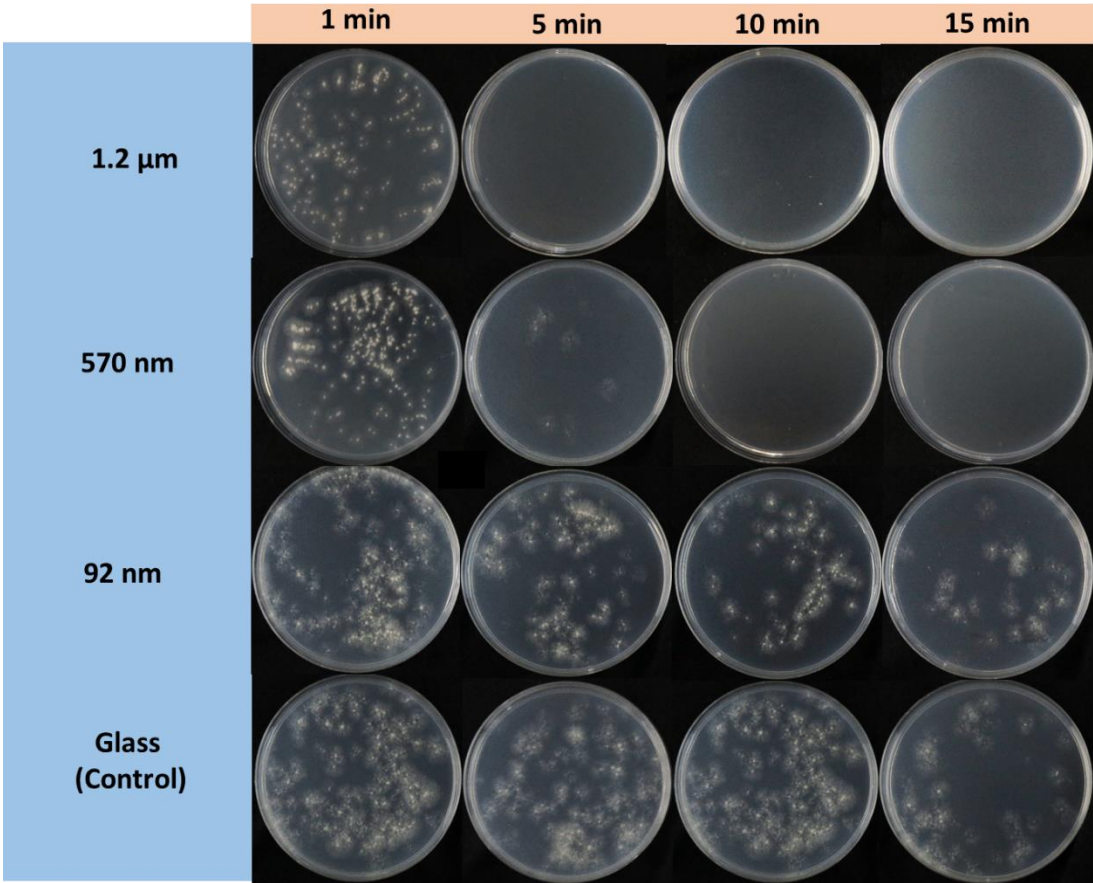
Fig. 4 Conidia growth of *C. gloeosporioides* for different Ag particle sizes and contact times.
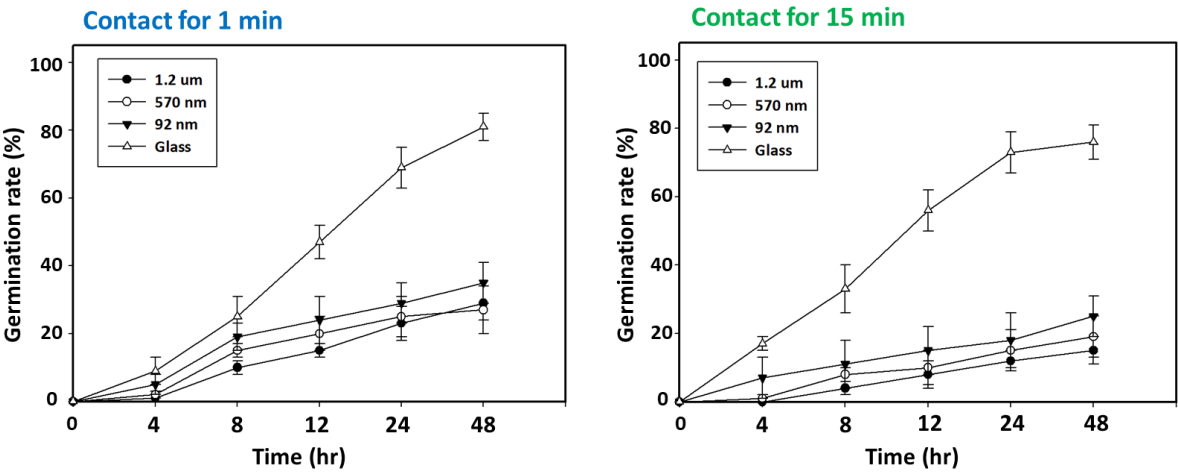
Fig. 5 Spore germination rate of *C. gloeosporioides* for different Ag particle sizes and contact times.
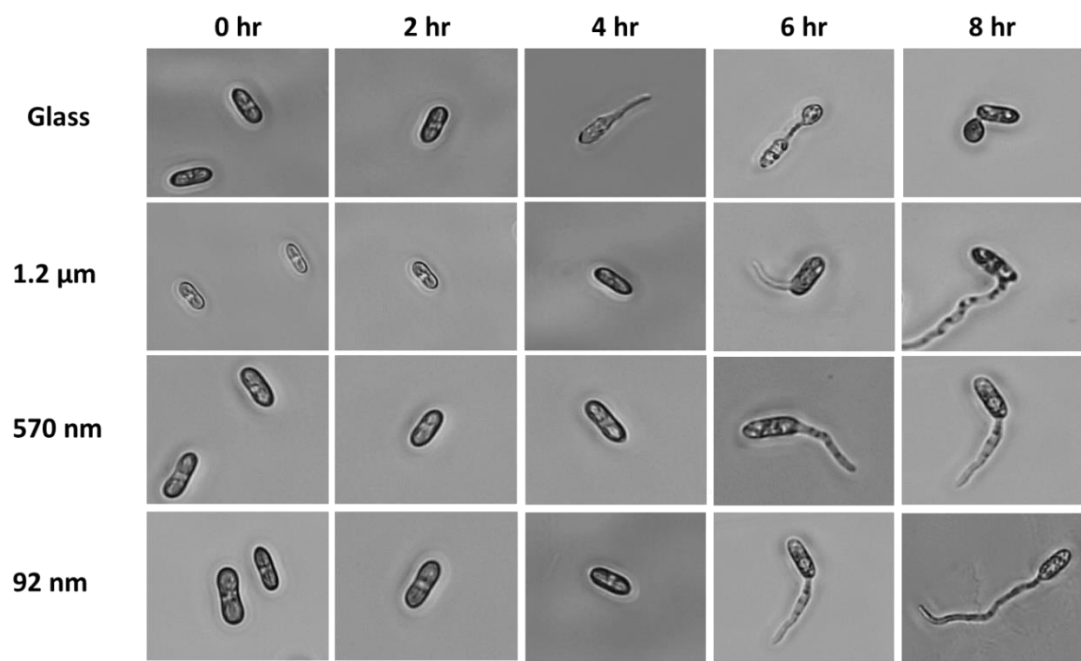
Fig. 6 Appressorium formation of *C. gloeosporioides* for different Ag particle sizes and contact times.
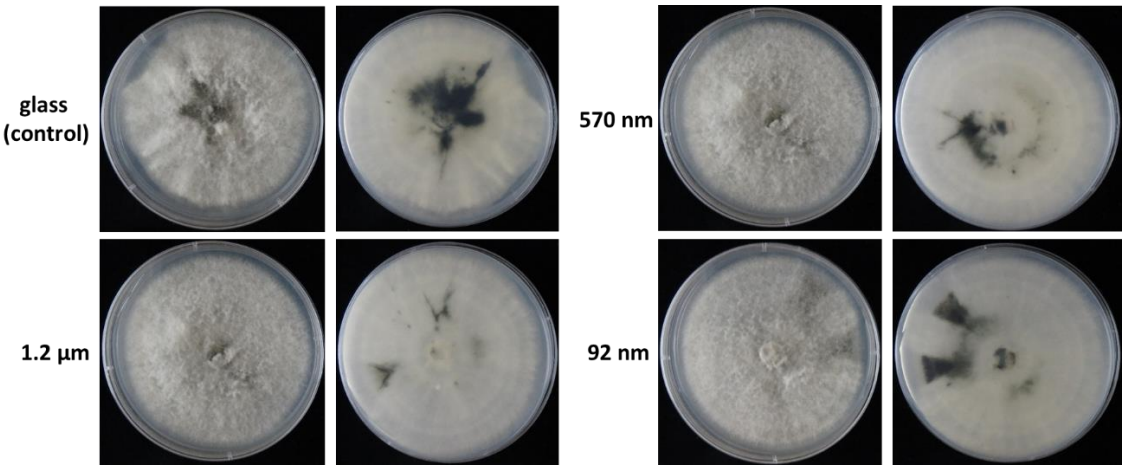
Fig. 7 Morphologies of *C. gloeosporioides* following treatment with different Ag samples.

Fig. 8 Relative expression of LAC1, PKS, THR, SCD, Ecg, and PEL genes following treatment with different Ag samples. *SR: internal reference 18s rRNA, LAC1: laccase gene, PKS: polyketide synthase gene, THR: tetra-HN reductase scytalone gene, SCD: scytalone dehydratase gene, Ecg: exo-glucocanase gene, and PEL: pectate lyase gene.

Fig. 9 Effects of Ag particle size on anthracnose of mango: (a) control, (b) 92 nm, (c) 570 nm, and (d) 1.2 μm.

Fig. 10 SEM micrographs of *C. gloeosporioides* treated with different Ag particle samples: (a) glass (control), and (b) 1.2 μm.

Fig. 1 SEM images of Ag particles with a size of: (a) 92 nm, (b) 570 nm, and (c) 1.2 μm.

Fig. 2 Cross-sectional images of Ag particles with different size of: (a) 92 nm, (b) 570 nm, and (c) 1.2 μm.

Fig. 3 Relationship between scanning speed and laser input energy for initial Ag film thickness of :
(a) 10 nm and (b) 50 nm.

Fig. 4 Conidia growth of *C. gloeosporioides* for different Ag particle sizes and contact times.

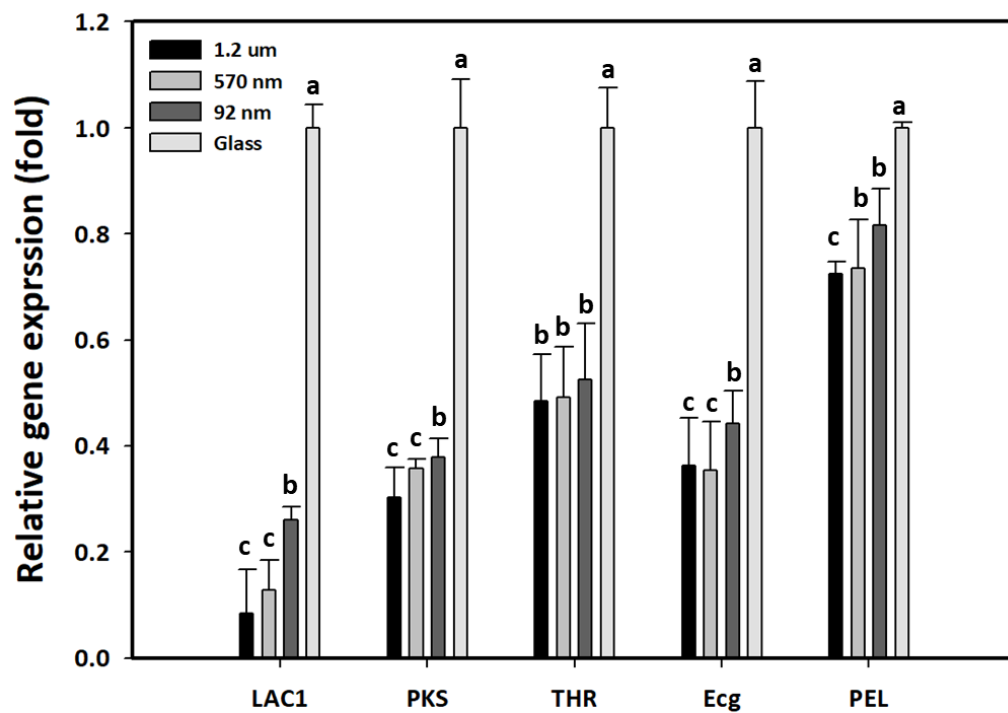Fig. 5 Spore germination rate of *C. gloeosporioides* for different Ag particle sizes and contact times.

Fig. 6 Appressorium formation of *C. gloeosporioides* for different Ag particle sizes and contact times.

Fig. 7 Morphologies of *C. gloeosporioides* following treatment with different Ag samples.

Fig. 8 Relative expression of LAC1, PKS, THR, SCD, Ecg, and PEL genes following treatment with different Ag samples. *SR: internal reference 18s rRNA, LAC1: laccase gene, PKS: polyketide synthase gene, THR: tetra-HN reductase scytalone gene, SCD: scytalone dehydratase gene, Ecg: exo-glucocanase gene, and PEL: pectate lyase gene.
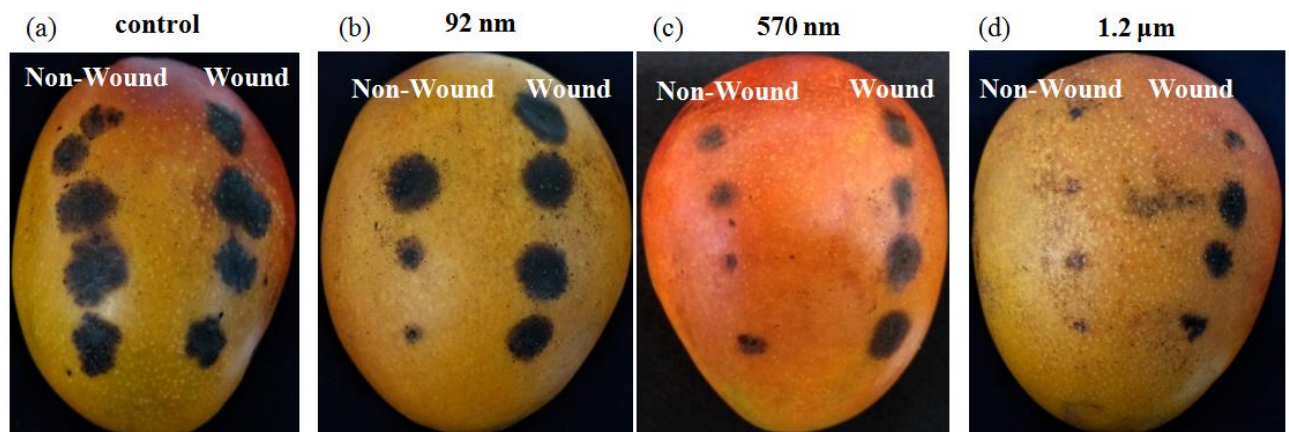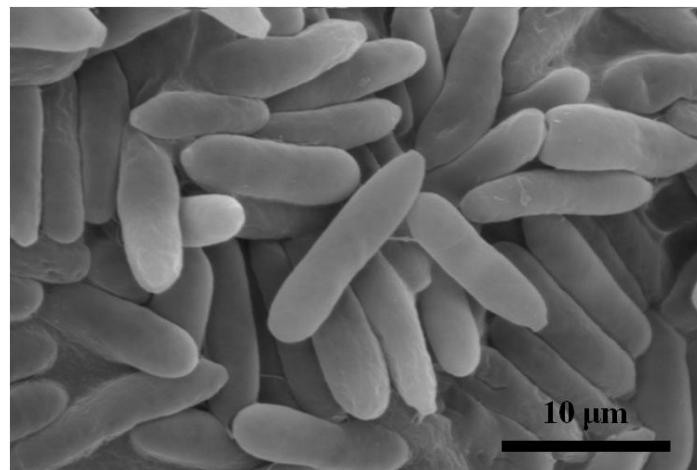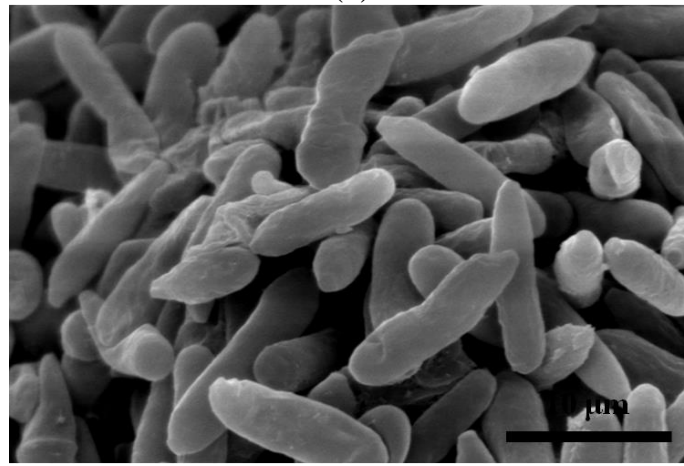

Fig. 9 Effects of Ag particle size on anthracnose of mango: (a) control, (b) 92 nm, (c) 570 nm, and (d) 1.2 μm.

(a)

(b)

Fig. 10 SEM micrographs of *C. gloeosporioides* treated with different Ag particle samples: (a) glass (control), and (b) 1.2 µm.